Journal of Mathematical Modeling
Vol. -, No. -, 2026, pp. -. Research Article

JMM

Bounded optimal feedback control of a fractional-order chaotic economic system

Seyed Reza Hejazi[†*], **Shaban Mohammadi**[†], **Mohammad Hossein Seifi**[†], **Elham Dastranj**[†]

[†]*Faculty of Mathematical Sciences, Shahrood University of Technology, Shahrood, Semnan, Iran*

Email(s): r_hejazi@shahroodut.ac.ir, arashmoh2019@gmail.com, mohammad.h.seifi@shahroodut.ac.ir, elham.dastranj@shahroodut.ac.ir

Abstract. We study bounded optimal feedback control of chaos in a fractional-order macroeconomic model. Two equilibria are index-two saddles, so the necessary condition for chaos holds for every commensurate order $\alpha > 0.8863$, yet numerically chaos appears only above $\alpha \approx 0.96$, after a period-doubling cascade; at $\alpha = 0.99$ the 0–1 test gives $K = +0.998$. A normalized quadratic cost about the positive equilibrium is minimized over saturated three-gain feedback laws with $u_{\max} = 0.05$, using a genetic algorithm and particle swarm optimization. Both reach $J = 244.8213$ and cut the index by $98.7\% \pm 1.1\%$ over an ensemble of initial conditions drawn from the attractor. A saturated linear-quadratic regulator comes within 0.03% of this optimum, and under the same bound the design beats active control by only 9% in state cost: equivalence, not superiority. Delay is the binding limitation, about a quarter of a time unit.

Keywords: Fractional-order model; chaotic economic system; optimal control; particle swarm optimization; genetic algorithm.
AMS Subject Classification 2010: 34C28, 49J20, 68W50.

1 Introduction

Chaotic behaviour is of interest in economics because it can explain how erratic movements of aggregate variables can be generated by a purely deterministic mechanism rather than by exogenous random shocks [8, 19, 40, 42]. Low-dimensional deterministic models reproduce irregular business-cycle and financial dynamics, and the identification and control of such behaviour has become a practical question for policy design [5, 8, 28, 51].

Fractional calculus provides a natural language for these models. A fractional derivative is non-local: the current rate of change of a state depends on the whole history of that state, which is the memory effect that aggregates such as savings or capital stock exhibit [28, 34, 37, 39]. Numerical methods for

*Corresponding author
Received: 30 August 2026/ Revised: 20 October 2026/ Accepted: 21 October 2026
DOI: 10.22124/jmm.2026.34789.3240

© 2026 University of Guilan

Corrected Proof

differentiation and integration of non-integer order have made fractional-order systems accessible to the control community [4, 7, 20]. A nonlinear system may retain chaotic behaviour when its integer-order derivatives are replaced by fractional ones [6,21,44], and such models have been used for digital circuits, ferroelectric materials, biological systems and economics [29,36,41,46].

Recent work has extended these models in several directions. Discrete fractional macroeconomic and financial systems have been analysed for bifurcation, chaos and complexity [1, 9, 15], variable-order formulations have been proposed together with identification schemes [48], chaos has been studied and controlled in fractional supply-chain models [24] and in modified financial systems [17], feedback control of fractional difference equations has been developed [25], and the 0–1 test has become a standard companion to the Lyapunov exponent [50]. Closest to the present work is [23], where a nonlinear model predictive controller is designed for a variable-order hyperchaotic economic system and the fractional optimal control problem is solved as a two-point boundary value problem.

Several control strategies have been applied to fractional-order chaotic systems. Active control has been applied to the three-dimensional fractional economic system of interest here [5], where chaos is asserted from phase portraits alone; sliding-mode and adaptive schemes have been applied to a four-dimensional hyperchaotic extension of it [51], with Lyapunov exponents and basins of attraction as evidence; and chaos control and synchronization have been studied for other fractional systems [22, 30]. Optimal control, in the sense of minimizing an explicit performance index, has been used for fractional and integer-order chaotic models in other application areas [18], and metaheuristics are an attractive way of solving the resulting problem when the cost is not differentiable in closed form and the admissible set is constrained. What is missing, and what motivates this paper, is an optimal-control formulation for the system of [5] in which (i) the performance index is stated explicitly, (ii) the control is bounded and of simple feedback form, and (iii) the design is compared, on the same model and with the same performance measures, against the active control previously proposed for that model.

The contribution is threefold. First, at the parameter values of [5] the three equilibria are computed and classified, and the necessary condition for a chaotic attractor yields the analytical lower bound $\alpha > 0.886305$ on the commensurate order; the dependence on the order above that bound is then studied numerically. Second, a well-posed optimal control problem is formulated: the performance index is normalized so that the three states, whose magnitudes differ by two orders of magnitude, contribute comparably, the control is bounded, and the admissible control is a saturated feedback law, so that the policy is continuous and robust rather than an open-loop sequence. Third, the problem is solved by a genetic algorithm and by particle swarm optimization, and the designs are placed against three references on a common footing: a deterministic local optimizer, the active control of [5] under the same amplitude bound, and a saturated linear-quadratic regulator. The outcome is one of equivalence rather than superiority, and we report it as such. The paper is therefore a simulation-based design procedure, not a new controller: unlike [5], it uses one bounded input and an explicit cost, and unlike the predictive controller of [23], it solves no optimization online; the three gains are fixed once, by minimizing the cost on the nonlinear fractional dynamics under the bound, subject to a local stability constraint at the target.

Section 2 collects the definitions and stability results used later. Section 3 presents the economic system, classifies its equilibria and locates its chaotic region, both analytically and numerically. Section 4 formulates the optimal control problem and describes the two metaheuristics and the deterministic benchmark used to solve it. Sections 5 and 6 report and discuss the numerical results, including the comparison with alternative controllers, the robustness tests and the basin of attraction.

Corrected Proof

2 Preliminaries and basic definitions

Definition 1. *The Riemann–Liouville fractional integral operator of order ν of a function $f(t) \in C_\mu$, $\mu \geq -1$, is*

$$I^\nu f(t) = \begin{cases} \dfrac{1}{\Gamma(\nu)} \displaystyle\int_0^t \frac{f(s)}{(t-s)^{1-\nu}} ds = \frac{1}{\Gamma(\nu)} t^{\nu-1} * f(t), & \nu > 0, \\ f(t), & \nu = 0, \end{cases} \tag{1}$$

where $t^{\nu-1} * f(t)$ is the convolution product, C_μ denotes the space of functions that can be written as $t^p f_1(t)$ with $p > \mu$ and f_1 continuous on $[0,\infty)$, and C_μ^n the space of functions whose n-th derivative lies in C_μ. The operator is linear and satisfies $(I^{\nu_1} I^{\nu_2} f)(t) = I^{\nu_1+\nu_2} f(t)$.

Definition 2. *The Caputo fractional derivative of order ν of a function $f(t) \in C_{-1}^n$ is*

$$D^\nu f(t) = \frac{1}{\Gamma(n-\nu)} \int_0^t \frac{f^{(n)}(s)}{(t-s)^{\nu+1-n}} ds, \quad n-1 < \nu < n,\ t > 0,\ n \in \mathbb{N}, \tag{2}$$

and $D^n f = f^{(n)}$ for $\nu = n$, so that $\alpha = 1$ in (10) gives the classical system. The Caputo derivative and the Riemann–Liouville integral satisfy $(D^\nu I^\nu f)(t) = f(t)$ and

$$(I^\nu D^\nu f)(t) = f(t) - \sum_{i=0}^{n-1} f^{(i)}(0) \frac{t^i}{i!}, \tag{3}$$

and further properties can be found in [26].

Throughout the paper D_t^α denotes the Caputo derivative with respect to t. A commensurate system is one in which all the derivative orders are equal; otherwise the system is called incommensurate. The two cases obey different stability conditions, as stated next.

2.1 Stability criterion

Theorem 1 (see [13, 32])**.** *Consider the autonomous linear fractional-order system*

$$D_t^\alpha x = Ax, \quad x(0) = x_0, \qquad x \in \mathbb{R}^n,\ A \in \mathbb{R}^{n\times n}. \tag{4}$$

i) For $0 < \alpha < 1$, system (4) is asymptotically stable if and only if $|\arg(\lambda)| > \frac{\alpha\pi}{2}$ holds for every *eigenvalue λ of A. It is stable if $|\arg(\lambda)| \geq \frac{\alpha\pi}{2}$ for every eigenvalue and those eigenvalues satisfying $|\arg(\lambda)| = \frac{\alpha\pi}{2}$ have geometric multiplicity one.*

ii) For the nonlinear commensurate system

$$D_t^\alpha x = f(x), \qquad f(x^*) = 0, \tag{5}$$

with $0 < \alpha < 1$ and $x \in \mathbb{R}^n$, the equilibrium x^* is locally asymptotically stable if every eigenvalue λ of the Jacobian matrix $\mathscr{J} = \left.\frac{\partial f}{\partial x}\right|_{x^*}$ satisfies [3, 32]

$$|\arg(\lambda)| > \frac{\alpha\pi}{2}. \tag{6}$$

Corrected Proof

For an incommensurate system $D_t^{\alpha_i} x_i = f_i(x_1,\ldots,x_n)$, $i = 1,\ldots,n$, with $0 < \alpha_i < 1$, the equilibria are again the solutions of $f_i = 0$ [38, 45], and the linearization about an equilibrium x^* is governed by the same Jacobian $\mathscr{J} = \partial f/\partial x|_{x^*}$ [44]. Writing $\alpha_i = v_i/q_i$ with $(v_i, q_i) = 1$ and $v_i, q_i \in \mathbb{Z}^+$, and letting M be the least common multiple of the q_i, the equilibrium is asymptotically stable provided $|\arg(\lambda)| > \pi/(2M)$ for every root λ of [13, 32, 33]

$$\det\Big(\operatorname{diag}\left([\lambda^{M\alpha_1}\ \lambda^{M\alpha_2}\ \ldots\ \lambda^{M\alpha_n}]\right) - \mathscr{J}\Big) = 0, \tag{7}$$

where $\operatorname{diag}([m_1\ \ldots\ m_n])$ is the $n \times n$ diagonal matrix with entries $m_1,\ldots,m_n$. In the commensurate case $\alpha_1 = \cdots = \alpha_n = \alpha$ one has $M = q_1$ and (7) reduces to the eigenvalue condition (6).

2.2 Required conditions for chaos in a fractional-order system

A saddle point of a three-dimensional integer-order system is an equilibrium with at least one eigenvalue in each open half-plane [31, 35]; it is of index one if exactly one eigenvalue is unstable, and of index two if two are [35]. A chaotic attractor of a three-dimensional system is organized around a saddle point of index two, and the same holds for the fractional-order counterpart [22].

Let $\dot{x} = f(x)$ be a three-dimensional system with a chaotic attractor and let Ω be the set of its equilibria surrounded by a scroll of the attractor [13]. The systems $D^\alpha x = f(x)$, with $D^\alpha \equiv (D_t^{\alpha_1}, D_t^{\alpha_2}, D_t^{\alpha_3})$, and $\dot{x} = f(x)$ have the same equilibria [13], so a *necessary* condition for $D^\alpha x = f(x)$ to possess a chaotic attractor is [43, 47]

$$\left(\frac{\pi}{2M}\right) - \min_i |\arg(\lambda_i)| > 0, \tag{8}$$

where the λ_i are the roots of $\det\left(\operatorname{diag}([\lambda^{M\alpha_1}\ \lambda^{M\alpha_2}\ \lambda^{M\alpha_3}]) - \partial f/\partial x|_{x^*}\right) = 0$ for all $x^* \in \Omega$. If all the equilibria of the system are stable, no trajectory tends to a chaotic attractor; moreover, even when (8) holds, only initial conditions lying in the basin of attraction produce chaotic trajectories [33]. In the commensurate case $\alpha_1 = \alpha_2 = \alpha_3 = \alpha$, condition (8) takes the simpler form [32, 43, 44]

$$\alpha > \frac{2}{\pi} \min_i |\arg(\lambda_i)|, \tag{9}$$

in which the λ_i are the eigenvalues of the Jacobian matrix $\left.\frac{\partial f}{\partial x}\right|_{x^*}$, the minimum being taken over the spectrum at a given x^*, and the condition being required to hold for at least one $x^* \in \Omega$. Both conditions are necessary and not sufficient, so the existence of a chaotic attractor must be established separately [10, 49].

3 The fractional-order economic system

3.1 The model

We study the three-dimensional fractional-order macroeconomic model with foreign capital investment introduced in [5],

$$\begin{aligned} D_t^\alpha x(t) &= a_1 y + a_2 x(a_3 - y^2), \\ D_t^\alpha y(t) &= -x + a_4 z, \\ D_t^\alpha z(t) &= a_5 x - a_6 y, \end{aligned} \tag{10}$$

Corrected Proof

Table 1: Parameters of model (10), with the values of [5]. The commensurate order is not taken from that work, which reports $\alpha = 0.9$; it is determined in Section 3.3, where $\alpha = 0.9$ is shown to give a periodic and not a chaotic attractor.

Parameter	a_1	a_2	a_3	a_4	a_5	a_6	α
Value	0.02	0.4	1	50	10	0.1	0.99

where $\alpha \in (0,1]$ and the state variables x, y and z denote, respectively, the savings of households, the gross domestic product (GDP) and the foreign capital inflow. The derivative is taken with respect to time, and the parameters are non-negative ratios: a_1 is the marginal propensity to save, a_2 the ratio of capitalized profit, a_3 the potential GDP, a_4 the output/capital ratio, a_5 the capital inflow/savings ratio and a_6 the debt refund/output ratio; their values are collected in Table 1. In the last equation the foreign capital inflow is coupled to savings through a_5 and to the debt-service burden on output through a_6, so the two terms act on different state variables.

3.2 Equilibria and their classification

The equilibria of (10) solve $a_1 y + a_2 x(a_3 - y^2) = 0$, $-x + a_4 z = 0$ and $a_5 x - a_6 y = 0$. The last two give $y = (a_5/a_6)x$ and $z = x/a_4$, and substitution into the first yields

$$x\left[a_1\frac{a_5}{a_6} + a_2 a_3 - a_2\left(\frac{a_5}{a_6}\right)^2 x^2\right] = 0. \tag{11}$$

Hence the origin is always an equilibrium, and two further real equilibria exist whenever $a_1 a_5/a_6 + a_2 a_3 > 0$, namely

$$x^* = \pm\frac{a_6}{a_5}\sqrt{\frac{a_1 a_5/a_6 + a_2 a_3}{a_2}}, \qquad y^* = \frac{a_5}{a_6}x^*, \qquad z^* = \frac{x^*}{a_4}. \tag{12}$$

System (10) is odd in the state, so the non-trivial equilibria come in a pair E_1 and $E_2 = -E_1$ with identical spectra, the attractor has two symmetric scrolls, and the control design for E_2 is that for E_1 with $u \mapsto -u$.

For the parameter values of Table 1 we obtain the three equilibria

$$E_0 = (0,0,0), \qquad E_1 = (0.024495,\ 2.449490,\ 4.898979\times 10^{-4}), \qquad E_2 = -E_1, \tag{13}$$

in agreement with [5]. The Jacobian matrix of (10) is

$$\mathscr{J}(x,y) = \begin{pmatrix} a_2(a_3 - y^2) & a_1 - 2a_2 xy & 0 \\ -1 & 0 & a_4 \\ a_5 & -a_6 & 0 \end{pmatrix}, \tag{14}$$

so that

$$\mathscr{J}|_{E_0} = \begin{pmatrix} 0.4 & 0.02 & 0 \\ -1 & 0 & 50 \\ 10 & -0.1 & 0 \end{pmatrix}, \qquad \mathscr{J}|_{E_1} = \mathscr{J}|_{E_2} = \begin{pmatrix} -2 & -0.028 & 0 \\ -1 & 0 & 50 \\ 10 & -0.1 & 0 \end{pmatrix}, \tag{15}$$

with characteristic polynomials $\lambda^3 - 0.4\lambda^2 + 5.02\lambda - 12$ at E_0 and $\lambda^3 + 2\lambda^2 + 4.972\lambda + 24$ at E_1 and E_2. The eigenvalues are 1.6762 and $-0.6381 \pm 2.5985\,i$ at E_0, a saddle of index one with $\min_i |\arg(\lambda_i)| = 0$, and -3.0042 and $0.5021 \pm 2.7815\,i$ at E_1 and E_2, saddles of index two with $\min_i |\arg(\lambda_i)| = 1.3922$.

Corrected Proof

Table 2: Transition range. Maxima: number of distinct local maxima of y in the second half of the $[0,2000]$ series (— when they do not cluster). K: 0–1 statistic for the three protocols P1 ($h=0.01$, $[0,1000]$), P2 ($h=0.005$, $[0,1000]$), P3 ($h=0.01$, $[0,2000]$). λ_T with $d_0=10^{-12}$, $t_{\mathrm{lo}}=20$

α	maxima	K_y, P1	K_y, P2	K_y, P3	K_x, P3	λ_T, $h=0.005$	λ_T, $h=0.0025$
0.940	1	−0.03	−0.02	−0.01	+0.01	−0.003	+0.000
0.945	1	−0.01	−0.01	−0.01	−0.01	−0.001	−0.004
0.950	2	−0.01	−0.01	−0.01	−0.01	−0.007	−0.004
0.955	2	−0.03	−0.03	+0.01	+0.00	−0.006	−0.002
0.9575	4	−0.04	−0.02	+0.01	+0.01	−0.012	−0.003
0.960	—	+0.34	+0.14	+0.33	+0.87	+0.096	+0.096
0.965	—	+0.99	+0.98	+0.99	+1.00	+0.200	+0.154
0.970	—	+1.00	+0.99	+1.00	+1.00	+0.273	+0.131

3.3 Chaotic region and choice of the order

Both E_1 and E_2 are saddle points of index two: each has one negative real eigenvalue and a complex conjugate pair with positive real part. By Section 2 these are the equilibria around which a chaotic attractor of a three-dimensional system can be organized, so $\Omega=\{E_1,E_2\}$, and (9) evaluated there gives

$$\alpha \;>\; \frac{2}{\pi}\,(1.3922052) \;=\; 0.886305, \tag{16}$$

the lower bound on the commensurate order for which chaotic behaviour of (10) is possible; the endpoint is excluded, since an eigenvalue on the boundary of the sector does not make the equilibrium unstable. We write 0.8863 for short below.

Because (9) is only necessary, we scanned the order over $[0.90,1.00]$ in steps of 0.005 by brute force, integrating each order separately from the initial condition of Section 3.4 with $h=0.005$ on $t\in[0,230]$; this samples trajectories and does not continue solution branches. Figure 2 records the local maxima of y for $t>120$, the divergence rate λ_T of Section 3.4 and, every 0.02, the 0–1 statistic of y sampled at unit intervals on $[100,230]$. These series are short, so the transition was rechecked at eight orders with three longer protocols, $h=0.01$ and $h=0.005$ on $[0,1000]$ and $h=0.01$ on $[0,2000]$, each discarding $t<200$ and sampling at unit intervals (801 or 1801 samples); Table 2 gives the result. There are three thresholds. The first is the analytical bound (16), below which chaos is impossible. The second is a period-doubling cascade: in the long series the maxima of y take one value up to $\alpha=0.945$, two at 0.950 and 0.955 and four at 0.9575, with $K\approx 0$ and $\lambda_T\le 3\times10^{-4}$. This is read from sampled trajectories, not from a converged continuation, so the doublings are located only to the spacing of the orders tested. The third is the onset of chaos. At $\alpha=0.960$ the maxima no longer cluster and $\lambda_T\approx 0.095$ for both steps and both d_0, but K is intermediate and depends on the protocol, from 0.14 to 0.34 for y and up to 0.87 for x; from $\alpha=0.965$ every protocol gives $K>0.98$. We therefore place the onset in the interval $(0.9575,0.965]$, a numerically estimated transition range rather than a resolved threshold.

Throughout the remainder of the paper we therefore fix the commensurate order $\alpha_1=\alpha_2=\alpha_3=\alpha=0.99>0.8863$, which lies inside the numerically identified chaotic band, although that band is not uniform: λ_T dips near $\alpha\approx0.985$ and $\alpha\approx0.995$, the usual signature of narrow periodic windows, so no claim of chaos for *every* order above 0.96 is made here. Since $\alpha=99/100$ is commensurate, $M=100$ and (9), the commensurate specialization of (8) rather than an alternative to it, may be used directly; for $\alpha=0.99$ one has $\alpha\pi/2=1.5551>1.3922$, so (6) is violated at E_1 and E_2 and these equilibria are

Corrected Proof

Table 3: Finite-time divergence rate λ_T at $\alpha = 0.99$ for two steps h, three initial separations d_0 and two fit starts t_{lo}; a dash means fewer than 300 samples in the fit range

	$d_0 = 10^{-12}$		$d_0 = 10^{-9}$		$d_0 = 10^{-6}$	
$h \setminus t_{\mathrm{lo}}$	20	30	20	30	20	30
0.005	0.336	0.348	0.302	0.484	0.003	—
0.0025	0.400	0.455	0.297	0.274	−0.033	—

unstable, as required. The gap between the analytical bound 0.8863 and the observed onset near 0.96 is a quantitative illustration of the fact that (9) identifies the orders for which chaos is possible, not those for which it occurs.

3.4 Numerical verification of chaos

Condition (16) is necessary only, so the presence of chaos is established by two independent diagnostics. All the simulations of this paper use the improved Adams–Bashforth–Moulton predictor–corrector scheme for fractional-order systems [16, 20], which is also the scheme used in [5], with step size $h = 0.005$ for the trajectories of this section ($h = 0.01$ for the long series of the 0–1 test) and initial condition $(x_0, y_0, z_0) = (1.1, -1.6, -1.3)$. Two numerical solutions of the same chaotic orbit agree on the statistics of the attractor but not pointwise, so the step was validated on those statistics: halving h to 0.0025 moves the root-mean-square values of (x, y, z) by 0.97%, 0.35% and 1.74%. The divergence rate λ_T below is far more sensitive to the step.

The first diagnostic is the 0–1 test of Gottwald and Melbourne, a standard companion to the Lyapunov exponent for fractional-order maps and flows [50]. The observable is y, sampled at unit intervals over $t \in [100, 1000]$, and the statistic K is the median over 25 random values of $c \in (\pi/5, 4\pi/5)$ of the correlation between the mean square displacement and the lag, with the oscillatory term removed. Our implementation returns $K = +0.999$ for the logistic map at $r = 4$ and $K = -0.004$ for a quasi-periodic signal, as expected. Applied to the model it gives $K = +0.998$ for y, $+0.997$ for x and $+0.997$ for z at $\alpha = 0.99$, and $K = -0.017$ at $\alpha = 0.9$. The statistic is stable for sampling intervals between 0.5 and 4 time units; at 0.25 the series is oversampled and the test loses its discriminating power, a known limitation of the test.

The second diagnostic is a finite-time divergence rate λ_T, the two-trajectory estimate of the largest Lyapunov exponent [49] (see [10] for fractional-order systems). A second trajectory starts from $(x_0 + d_0, y_0, z_0)$ and is integrated with the same scheme, with its own full memory from $t = 0$; there is no renormalization and no repeated perturbation. λ_T is the least-squares slope of $\log d(t)$, d being the Euclidean distance between the two trajectories, over all samples of $t \in [t_{\mathrm{lo}}, 110]$ with $d < 10^{-2}$. Table 3 gives it for two steps, three values of d_0 and two values of t_{lo}. With $d_0 \le 10^{-9}$ it is positive, between 0.27 and 0.48, but it changes by up to 60% with the settings; with $d_0 = 10^{-6}$ the separation reaches 10^{-2} by $t \approx 21$ and the fit sees only the saturated regime. Without renormalization λ_T is not a converged Lyapunov exponent, so only its sign is used, and the 0–1 test is the primary evidence. Figure 2 uses $h = 0.005$, $d_0 = 10^{-12}$ and $t_{\mathrm{lo}} = 20$.

Neither diagnostic detects a transient: the spread of the local maxima of y over $[100, 300]$, $[300, 500]$, $[500, 700]$ and $[700, 1000]$ is 7.03, 7.70, 7.75 and 7.89. Figure 1 shows the attractor for $\alpha = 0.99$; its two scrolls, around E_1 and E_2, are separated along the savings axis.

Corrected Proof

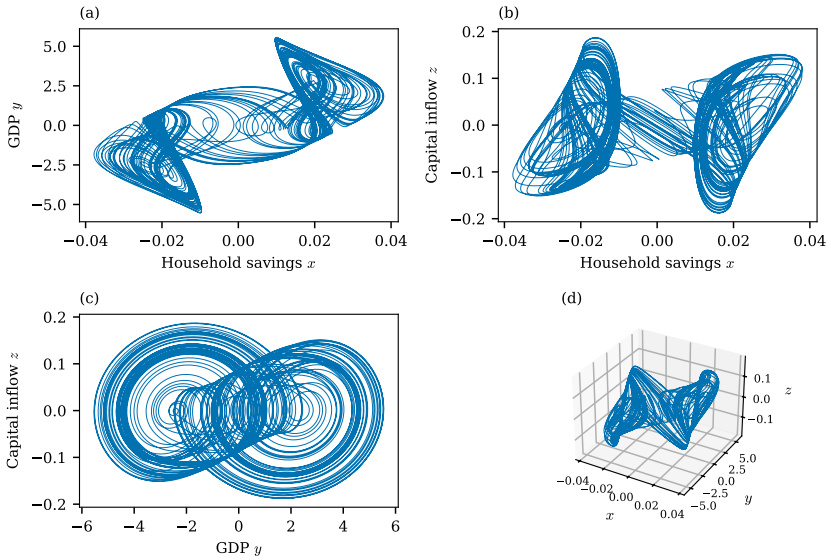

Figure 1: Phase portraits (a) x–y, (b) x–z, (c) y–z and (d) the three-dimensional chaotic attractor of (10) for $\alpha = 0.99$ and the parameters of Table 1, over $t \in [100, 400]$

The normalization constants of the performance index are fixed here for the rest of the paper. Measured over $t \in [100, 400]$, the root-mean-square values of the three states on the attractor are 0.0194, 2.60 and 0.0848 to three significant figures. We *define*

$$\sigma = (\sigma_x, \sigma_y, \sigma_z) = (0.0197,\ 2.57,\ 0.0818) \tag{17}$$

as fixed constants of the problem of Section 4. They are an earlier measurement of the same quantities and differ from the values above by at most 3.6%; re-estimating σ on another window or machine changes J by about 2%, more than any difference between the two algorithms, so fixing it makes J exactly reproducible.

The initial condition above lies in a basin of attraction that is not large; Section 5.6 returns to this.

4 The optimal control problem

4.1 Controlled system, target and controllability

A scalar policy instrument $u(t)$ is introduced into the model. It is scalar, but it is not confined to one equation: it enters all three through the distribution vector b, with its largest effect on the savings channel.

$$\begin{aligned} D_t^{\alpha} x(t) &= a_1 y + a_2 x(a_3 - y^2) + b_1 u(t), \\ D_t^{\alpha} y(t) &= -x + a_4 z + b_2 u(t), \\ D_t^{\alpha} z(t) &= a_5 x - a_6 y + b_3 u(t), \end{aligned} \tag{18}$$

with the distribution vector $b = (b_1, b_2, b_3)^T = (1, -0.5, -0.5)^T$. The vector encodes the economic reading of the instrument: it acts mainly on household savings and, with half the weight and the opposite

Corrected Proof

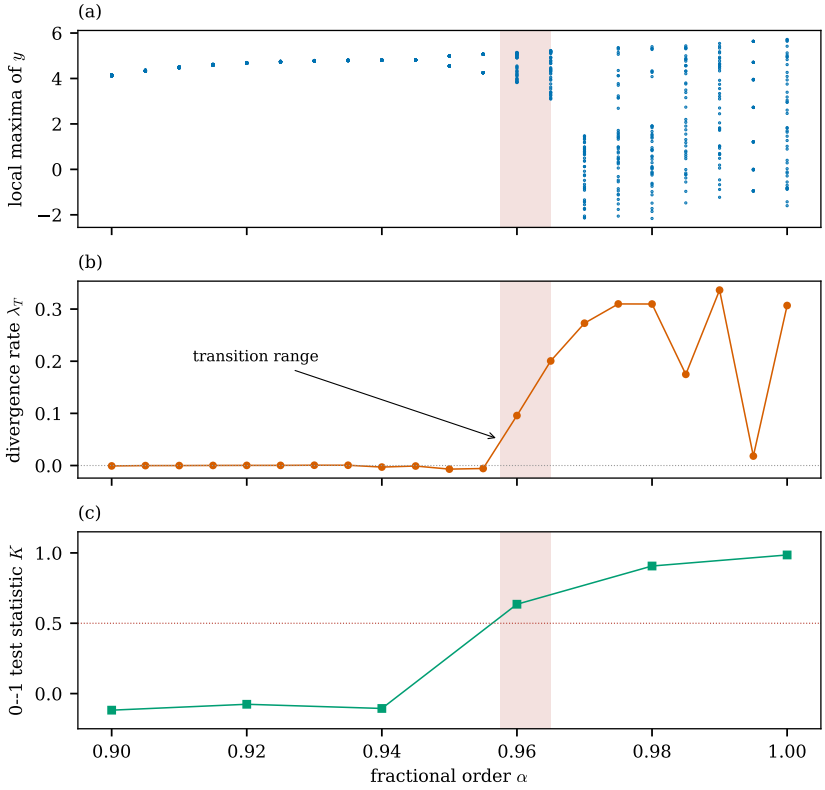

Figure 2: (a) Local maxima of y on the attractor against the commensurate order α; (b) divergence rate λ_T; (c) statistic K of the 0–1 test, decision level $K = 0.5$ dotted. Panel (c) uses the same, shorter trajectories as (a) and (b), so it is noisier near the transition; Table 2 repeats the test with longer series. The shaded band is the transition range $(0.9575, 0.965]$ of Table 2; condition (16) already holds from $\alpha = 0.8863$, and the interval between the two is the gap discussed in Section 3.

sign, on output and on the capital inflow, as a savings incentive would, since part of the extra saving comes out of current spending and replaces foreign capital. It was fixed on this reading before any cost was computed; it is not an optimum. Keeping the gains fixed and varying b, the cost on $t \in [0, 100]$ is 244.68 for $(1, -0.5, -0.5)$, 244.12 for $(1, 0, 0)$, 246.47 for $(1, -1, -1)$ and 244.03 for $(1, 0.5, 0.5)$, and (A, b) is controllable in all four cases. Two alternatives are therefore cheaper, by at most 0.27%. We keep the adopted vector because choosing b by the value of J would turn a modelling assumption into a design variable fitted to the index, and because every design compared in Section 5 uses the same b.

The control is to suppress the chaotic oscillations and drive the economy to a stationary regime. The origin E_0 is not an admissible target, since zero savings and zero output carry no economic meaning and E_0 is itself an unstable saddle; we therefore take the positive equilibrium $X^* = (x^*, y^*, z^*) = E_1 = (0.024495,\ 2.449490,\ 4.898979 \times 10^{-4})$ as the target state. Linearizing (18) about X^* gives the pair (A, b) with $A = \mathscr{J}|_{E_1}$ from (15). The controllability matrix $[b \ \ Ab \ \ A^2 b]$ has determinant -4187.9 and full rank 3, so the linearized system is controllable and the target is reachable with the single instrument chosen. Because E_1 is a saddle point of index two, the feedback must move the unstable pair into the

stable sector of the fractional-order system, that is, every eigenvalue λ of the closed-loop matrix must satisfy $|\arg(\lambda)| > \alpha\pi/2 = 1.5551$. This condition is imposed on the linearization at X^* and guarantees local asymptotic stability of the target only (Theorem 1(ii)); it says nothing about initial conditions far from X^*, which are examined numerically in Section 5.6.

4.2 Performance index

The three states of (10) differ by up to two orders of magnitude on the attractor, so an unweighted quadratic cost would be dominated by y and would effectively ignore x and z. Each state deviation is therefore normalized by its root-mean-square value $\sigma_x, \sigma_y, \sigma_z$ over the uncontrolled attractor, and the control effort is normalized by its bound. The performance index is

$$J = \int_0^{t_f} \left[\frac{(x-x^*)^2}{\sigma_x^2} + \frac{(y-y^*)^2}{\sigma_y^2} + \frac{(z-z^*)^2}{\sigma_z^2} + \rho \frac{u^2}{u_{\max}^2} \right] dt, \tag{19}$$

subject to the dynamics (18), the initial condition of Section 3.4, and the amplitude constraint

$$|u(t)| \le u_{\max}, \quad t \in [0, t_f]. \tag{20}$$

The normalization constants are those defined in (17) and the horizon is $t_f = 400$. The control weight is $\rho = 1$, which after the normalization of both terms is a scaling convention rather than a design choice: varying ρ from 0.1 to 10 with the gains held fixed leaves the state cost at 243.10 and the control energy at 3.95×10^{-3} and merely shifts J. The bound is set to $u_{\max} = 0.05$, which is 2.48 times the root-mean-square value 0.0201 of the right-hand side of the savings equation on the uncontrolled attractor: the instrument is allowed an authority of the same order as the intrinsic dynamics of that channel. The model is dimensionless, so the bound is best judged against the scale of the states: it is about 2.5 times the root-mean-square size $\sigma_x = 0.0197$ of the savings fluctuations and about 2% of the equilibrium output $y^* = 2.449$, enough to steer the savings flow but far too small to dominate the economy. The quadratic form of (19) is standard [27]. For fractional-order dynamics the necessary conditions of optimality involve left and right fractional derivatives [2], a route followed in [23]; that two-point boundary value problem is not solved here.

4.3 Parameterization of the admissible control

Optimizing the samples of $u(t)$ independently produces a control that changes sign at every step. Such a signal has no plausible reading as a policy, is penalized by the term ρu^2 in (19), and, being open-loop, is not robust on a system with exponential sensitivity to initial conditions. We therefore restrict the admissible controls to a saturated linear feedback law, written in the same normalized coordinates as the cost: with $e_i = (X_i - X_i^*)/\sigma_i$,

$$u(t) = \mathrm{sat}_{u_{\max}}\Big(-u_{\max} \sum_{i=1}^{3} g_i\, e_i(t) \Big), \qquad \mathrm{sat}_c(v) = \max\{-c, \min\{c, v\}\}, \tag{21}$$

so that the decision vector is the triple of dimensionless gains $\theta = (g_1, g_2, g_3)$ and the corresponding physical gains, in the units of the states, are

$$k_i = \frac{u_{\max}\, g_i}{\sigma_i}, \qquad u(t) = \mathrm{sat}_{u_{\max}}\big(-k^T (X - X^*) \big). \tag{22}$$

Corrected Proof

Both forms are reported in Section 5; the normalized form is what the optimizer searches over and the physical form what a user of the model would implement. The optimal control problem becomes the finite-dimensional program

$$\min_{\theta\in\Theta} J(\theta), \qquad \Theta = \Big\{\theta : \ |g_i| \le g_{\max}, \ \ \big|\arg\lambda_j(A-bk^T)\big| > \tfrac{\alpha\pi}{2} \ \ \forall j\Big\}, \tag{23}$$

with $g_{\max} = 8$. The second constraint is the fractional stability sector at the target. It is imposed by a penalty: every algorithm below minimizes

$$F(\theta) = J(\theta) + \Pi\,\mathbf{1}[\theta \notin \Theta_s], \qquad \Pi = 10^4, \tag{24}$$

where Θ_s is the set of gains that satisfy the sector condition, $\mathbf{1}$ is the indicator function, and $J(\theta)$ is always obtained by integrating (18), a non-finite value being replaced by 10^{12}. The penalty is added to J, so F is not constant on the infeasible set, but Π is more than an order of magnitude above the largest admissible value of J, so an infeasible design is never competitive. Two consequences follow. First, 78% of a uniformly random population lies outside Θ, averaged over the thirty initial populations actually used, so the constraint is active rather than decorative. Second, the penalty term is a step of fixed height Π at the boundary of Θ_s: it does not grow with the size of the violation, so it gives no graded measure of how far an infeasible design is from Θ_s. This does not make F flat outside Θ_s, where it still varies with J. A penalty growing with the violation, such as $\Pi\sum_j \max\{0, \alpha\pi/2 - |\arg\lambda_j|\}$, would provide such a measure and is the natural refinement. Each evaluation of $J(\theta)$ costs one integration of (18).

4.4 Genetic algorithm, particle swarm optimization and a deterministic benchmark

Problem (23) is solved with a genetic algorithm (GA) and with particle swarm optimization (PSO). In the GA, each chromosome encodes the three gains as real numbers, and selection, crossover and mutation are applied with elitism until the stopping rule is met. In PSO, each particle stores its position θ, its velocity and its personal best, and the swarm is updated with the inertia weight w and the cognitive and social coefficients c_1 and c_2. Both are executed in 30 independent runs with different random seeds so that the results can be compared statistically [14]; the settings are given in Table 4. The search runs on the reduced window $t \in [0, 20]$ with $h = 0.01$, which is cheap enough for 744 evaluations per run; every value of J reported in Section 5 is then obtained by re-integrating the design with $h = 0.0025$. Restricting the window from $[0, 400]$ to $[0, 20]$ changes J by 0.0004%, because the integrand has decayed long before $t = 20$: at $h = 0.0025$ the index is 244.8213 on $[0, 20]$, 244.8221 on $[0, 100]$ and 244.8223 on $[0, 400]$. Refining the step changes it more; on $[0, 20]$ the index is 244.0334, 244.6753, 244.8213 and 244.8559 at $h = 0.01$, 0.005, 0.0025 and 0.00125. The scheme converges at order 2.1 and Richardson extrapolation from the two finest steps gives $J \to 244.8667$, so at $h = 0.0025$ the remaining discretization error is 0.019%, which is the accuracy of every value of J quoted below.

As a benchmark we also solve (23) with a deterministic local optimizer, the Nelder–Mead simplex, applied to (24) with θ clipped to the box $|g_i| \le 8$ and started from six points drawn uniformly from that box, five of which lie outside Θ_s. The run started inside Θ_s converges to the optimum of the metaheuristics, to three decimal places; one run started outside reaches Θ_s at the edge of the box, at a cost 0.2% higher. The other four never evaluate a feasible point. They do not stop for lack of variation, since J ranges from 308 to 569 over their evaluations: for such gains the closed loop keeps oscillating irregularly, J is an irregular function of θ, with 3 to 43 local minima along a line of length 2 through each end

Corrected Proof

Table 4: Settings of the two metaheuristic algorithms and of the numerical integration. Both searches use 744 evaluations per run.

Genetic algorithm		*Particle swarm optimization*	
population size	24	swarm size	24
generations	30	iterations	30
selection	binary tournament	inertia weight w	$0.9 \to 0.4$ linear
crossover type / rate	BLX-0.5 / 1.0	coefficients c_1, c_2	1.5, 1.5
mutation type / rate	Gaussian, $\sigma = 1.6$ / 0.2	velocity bound	20% of the range
elite count	2		
Common settings: gain bound $g_{\max} = 8$ on the normalized gains; stopping criterion, generation budget; 30 independent runs, seeds 1000–1029 (GA) and 2000–2029 (PSO); Adams–Bashforth–Moulton integration [16, 20]; step by stage: $h = 0.01$ on $t \in [0, 20]$ for every evaluation of (24) (GA, PSO, Nelder–Mead, Figure 3); $h = 0.0025$ for every value reported in Section 5, robustness, noise and delay included; $h = 0.005$ for Section 3, the basin, and the sensitivity to b and ρ; $h = 0.01$ for the 0–1 series.			

point, and the simplex contracts onto one of them. A random population of 24 contains about five feasible members, so both metaheuristics start inside Θ_s. The four failures are consistent with an irregular J outside Θ_s combined with a penalty that gives no graded measure of the violation, but six starts do not show that either is the sole cause. The 1-in-6 success rate, against 30-in-30 for both population-based methods, is therefore empirical support for a population-based search on this problem, not a proof that one is needed. All computations use a Python 3.11 implementation with NumPy and SciPy and the fixed seeds of Table 4.

5 Numerical results

Every value of J in this section is obtained with $h = 0.0025$ and is therefore accurate to 0.019%; the exceptions are Figure 3, which shows the search values at $h = 0.01$, the segment variation of Section 5.3 ($h = 0.005$) and the basin ($h = 0.005$). Unless stated otherwise the evaluation window is $t \in [0, 400]$ for the nominal comparisons and $t \in [0, 100]$ for the baseline and robustness studies, and the error measures are

$$\mathrm{RMS} = \left(\frac{1}{T} \int_0^T \sum_i e_i^2 \, dt \right)^{1/2}, \quad \mathrm{IAE} = \int_0^T \sum_i |e_i| \, dt, \quad e_i = \frac{X_i - X_i^*}{\sigma_i}, \tag{25}$$

so that both depend on the window and must be quoted with it.

5.1 Uncontrolled dynamics and the baseline

The uncontrolled time histories at $\alpha = 0.99$ are the dotted curves of Figure 4. A baseline from the single initial condition $(1.1, -1.6, -1.3)$ is dominated by the excursion from that point, so we use an ensemble: 20 initial conditions sampled along the attractor at $t = 120, \ldots, 390$, each integrated for $t \in [0, 100]$. The uncontrolled ensemble gives $J = 549.5 \pm 81.7$ and $\mathrm{IAE} = 330.4 \pm 32.2$, and the same ensemble under the feedback of Section 5.2 gives $J = 7.0 \pm 5.9$ and $\mathrm{IAE} = 6.0 \pm 3.9$, so the reduction is $98.7\% \pm 1.1\%$ in J and $98.2\% \pm 1.2\%$ in IAE. The members are sampled from a chaotic orbit and differ between machines;

Corrected Proof

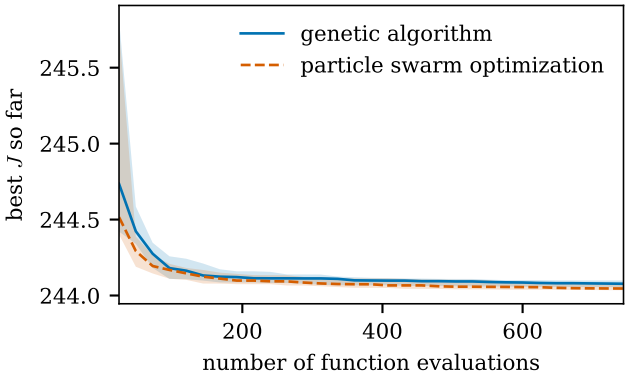

Figure 3: Convergence of the performance index (19) for the genetic algorithm and for particle swarm optimization; median over 30 independent runs, shaded area is the interquartile range. The vertical axis is linear, with plain decimal labels.

a different sample moves both reductions within 97% to 99%, and it is that band, not the third digit, that the ensemble establishes.

5.2 Convergence of the two algorithms and controlled response

Figure 3 reports the evolution of the best value of J against the number of function evaluations for both algorithms, as the median over the 30 runs with the interquartile band.

The gains returned by the two algorithms, in the normalized form of (21) and in the physical form of (22), are $\theta_{\mathrm{GA}} = (1.3988, -1.1280, 1.4773)$ with $k_{\mathrm{GA}} = (3.5503, -0.0219, 0.9030)$, and $\theta_{\mathrm{PSO}} = (1.3498, -1.1885, 1.4056)$ with $k_{\mathrm{PSO}} = (3.4258, -0.0231, 0.8592)$. The closed-loop eigenvalues at the target are -3.8645 and $-0.6226 \pm 2.9303\,i$ for the genetic algorithm, whose arguments π and 1.7802 both exceed $\alpha\pi/2 = 1.5551$, so the target is locally asymptotically stable. Figures 4 and 5 show the trajectories and the control signals. The signal is continuous, respects the bound (20) and vanishes as the state approaches the target; it is saturated only on $t \in [0, 0.91]$, that is on 4.6% of the optimization window, so saturation shapes the initial transient but does not drive the steady behaviour.

5.3 Performance and statistical comparison

Table 5 reports the two designs. Both reach the same best value of J to four decimal places. Over the 30 runs the difference of the means is 0.0178, that is 0.0073% of J, in favour of particle swarm optimization; the Mann–Whitney rank-sum test, appropriate because the runs are independent rather than paired [14], gives $U = 623$ and $p = 0.0108$, with Vargha–Delaney $\hat{A}_{12} = 0.692$ and rank-biserial correlation $r = +0.384$.

The difference is real but immaterial. It is 46 times smaller than the discretization error of the search step $h = 0.01$ at which the optimizer ranked the candidates, and its sign is not preserved by that step: at $h = 0.01$ the best particle-swarm design has the lower cost, at every finer step the best genetic-algorithm design does. The geometry shows why: the two gain vectors differ by 4.55%, and along the segment joining them J varies by 2×10^{-4} per cent, so the optimum is a flat valley rather than a well.

Corrected Proof

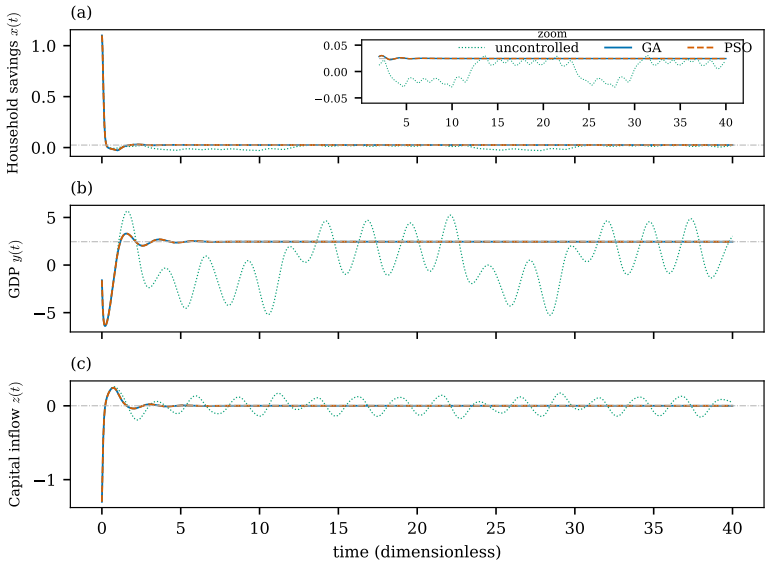

Figure 4: Controlled (solid and dashed) and uncontrolled (dotted) time histories of (a) x, (b) y and (c) z. Colour and line style both distinguish the curves, so the figure remains legible in greyscale; the inset zooms on the savings channel after the initial excursion

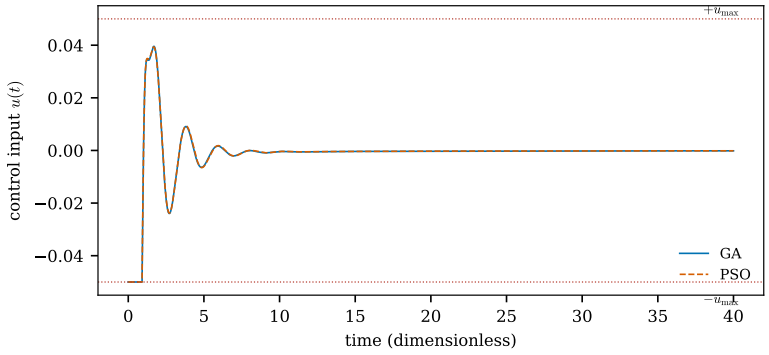

Figure 5: Control signal $u(t)$ of the two designs; the horizontal lines mark the amplitude bound $\pm u_{\max}$ of (20). The signal is saturated only on $t \in [0, 0.91]$.

The settling time depends on the threshold used. The initial normalized deviation is $|e(0)| = 56.9$; the time after which $|e(t)|$ stays below 2% of that value for the rest of the window is 1.34, and below the absolute levels 1, 0.2, 0.05 and 0.02 it is 1.37, 3.33, 5.42 and 6.92. The first is the conventional definition.

5.4 Comparison with alternative controllers

Table 6 compares the optimized feedback with three alternatives on the same model, initial condition and window. Two are the active control of [5], in the three-input feedback-linearizing form $v = -f(X) -$

Table 5: Performance of the two designs. Statistics of J over 30 independent runs on $t \in [0,20]$; all other entries for the best design of each algorithm on $t \in [0,400]$, with (25); $h = 0.0025$. Settling time: the time after which $|e(t)|$ stays below 2% of $|e(0)|$, as defined below.

Measure	GA	PSO	Measure	GA	PSO
best J	244.8213	244.8213	RMS	0.7798	0.7798
mean $\pm$ std	244.8645 ± 0.0313	244.8467 ± 0.0301	IAE	15.69	15.72
worst J	244.9282	244.9261	max $\lvert u \rvert$	0.0500	0.0500
state cost	243.24	243.24	$\int u^2 dt$	3.95×10^{-3}	3.95×10^{-3}
evaluations/run	744	744	settling time	1.34	1.34

Table 6: Comparison with alternative controllers, every entry on $t \in [0,100]$, same model and initial condition, $h = 0.0025$. A dash means the quantity is not reported: for Nelder–Mead only the objective is recorded, and for the active-control laws J and the IAE are not comparable, since those laws act through three inputs and do not minimize (19).

Controller	inputs	J	state cost	IAE	peak effort	energy
optimized feedback, GA	1 bounded	244.822	243.24	15.51	0.0500	3.95×10^{-3}
optimized feedback, PSO	1 bounded	244.822	243.24	15.54	0.0500	3.95×10^{-3}
Nelder–Mead (1 of 6 starts)	1 bounded	244.821	—	—	—	—
saturated LQR	1 bounded	244.888	243.16	15.25	0.0500	4.31×10^{-3}
active control, saturated	3 bounded	—	265.32	—	0.087	0.169
active control, unbounded	3 unbounded	—	1618.29	—	70.84	2510.4

$\lambda(X - X^*)$ with $\lambda = 1$, evaluated without a bound and with each channel saturated at the same $u_{\max} = 0.05$ used here. The third is the linear-quadratic regulator from the Riccati equation for the pair (A,b) of Section 4 with the weights of (19), that is $Q = \mathrm{diag}(\sigma_i^{-2})$ and $R = \rho / u_{\max}^2$, saturated at $u_{\max}$; its gains are $k_{\mathrm{LQR}} = (3.8305, -0.0373, 0.9086)$.

The comparison does not support a claim of superiority. Against unbounded active control the optimized feedback is better on every measure, but that comparison is not informative: the unbounded law is allowed a peak effort of 70.8 against 0.05, so the two are not solving the same problem. Under the same bound, active control attains a state cost of 265.3 against 243.2, that is 9% worse rather than the factor of six the unbounded comparison suggests. Against the saturated LQR the optimized feedback is not better at all: the LQR is 0.03% worse in J, the quantity being minimized, but better in state cost (243.16 against 243.24) and in IAE (15.25 against 15.51). Sixty runs of a stochastic search, at 744 evaluations each, therefore reproduce what one Riccati solution delivers in closed form. What the optimized feedback does offer is threefold: it evaluates the cost on the nonlinear model, with the linearization entering only through the stability constraint, and needs no Riccati equation; the bound $u_{\max}$ enters the design rather than being imposed afterwards on an unconstrained law; and the procedure applies unchanged to cost functionals with no closed-form solution.

5.5 Robustness

Table 7 reports the performance index on $t \in [0,100]$ under parameter perturbation, measurement noise, implementation delay and a change of initial condition. Each row carries the uncontrolled value for the same perturbation, without which the numbers invite the wrong conclusion: under $a_i \to 0.9a_i$ the

Corrected Proof

Table 7: Sensitivity of the performance index on $t \in [0,100]$, $h = 0.0025$, with the uncontrolled value for the same condition. A lower value than nominal is an improvement. The two designs agree to the digits shown in the nominal, the two parameter-perturbation and the $\tau = 0.1$ rows; those entries are equal, not copied.

Condition	uncontrolled	GA	PSO
nominal	662.41	244.82	244.82
$a_i \to 1.1\,a_i$	735.60	223.91	223.91
$a_i \to 0.9\,a_i$	802.36	270.67	270.67
noise 1% of σ, 20 seeds	662.41	244.876 ± 0.001	244.874 ± 0.001
noise 5% of σ, 20 seeds	662.41	246.164 ± 0.011	246.115 ± 0.011
delay $\tau = 0.1$	662.41	245.09	245.09
delay $\tau = 0.2$	662.41	246.42	246.37
delay $\tau = 0.25$	662.41	290.06	257.14
delay $\tau = 0.3$	662.41	1576.9	1594.1
initial condition $(0.3, 1.5, 0.5)$	–	543.91	544.68

controlled cost rises by 10.6%, but the uncontrolled cost for that parameter set rises by 21.1%, so relative to its own baseline the controller performs slightly better, not worse. The uncontrolled column, computed on a chaotic orbit, is reproducible to about ten per cent. The tests are defined as follows. In the parameter rows all six a_i are scaled together, while the gains, the target X^* and σ keep their nominal values; J therefore also counts the offset between X^* and the shifted equilibrium, 0.013 in normalized units, which adds less than 0.02 to J. In the noise rows the controller receives $X + \eta$ instead of X, with η_i Gaussian, of mean zero and standard deviation 1% or 5% of σ_i, drawn independently for each state and each step $h = 0.0025$ and held over the step; J uses the true state and the applied control, and the rows give the mean and standard deviation over 20 realizations. With delay the control is $u(t) = \mathrm{sat}_{u_{\max}}(-k^T(X(t-\tau) - X^*))$, with $X(t-\tau) = X(0)$ for $t < \tau$; a design fails if the mean of $|e|$ over $t \in [90,100]$ exceeds 0.05.

Implementation delay is the one genuine limitation. The design tolerates $\tau \le 0.2$ with a degradation below 0.7%; at $\tau = 0.25$ it still stabilizes but the cost rises by 18.5%; at $\tau = 0.3$ it fails and the cost exceeds twice the uncontrolled value (the mean of $|e|$ over $[90,100]$ is 0.001 at $\tau = 0.25$ and 3.6 at $\tau = 0.3$). The margin is between 0.25 and 0.3 time units, about one eighth of the dominant closed-loop period $2\pi/2.93 \approx 2.14$. Delay is also the only condition under which the two designs differ appreciably, by 13% at $\tau = 0.25$.

5.6 Basin of attraction

The results above all start from initial conditions on or near the attractor. Figure 6 shows how restrictive that is. Initial conditions on the slice $z_0 = -1.3$, $x_0 \in [-2,2]$, $y_0 \in [-4,4]$ were integrated with $h = 0.005$ on $t \in [0,50]$, with and without the GA feedback; a trajectory is labelled divergent when a component of the state reaches 10^3 in modulus, and bounded otherwise. Every divergent trajectory escapes before $t = 2.5$, and every bounded closed-loop trajectory ends within 0.05 of X^* in normalized distance. On the 9×9 grid of Figure 6, with spacing 0.5 in x_0 and 1 in y_0, only 28 of 81 points, that is 35%, remain bounded, the region is strongly asymmetric in x_0, and the initial condition used throughout sits close to its boundary. The closed loop gives the same 28 points. On a 41×41 grid, with spacing 0.1 and 0.2, the counts are 576 without and 574 with the feedback, out of 1681; the two maps differ at 8 points, all next to the boundary, 3 bounded only with the feedback and 5 only without it. The feedback thus changes

Corrected Proof

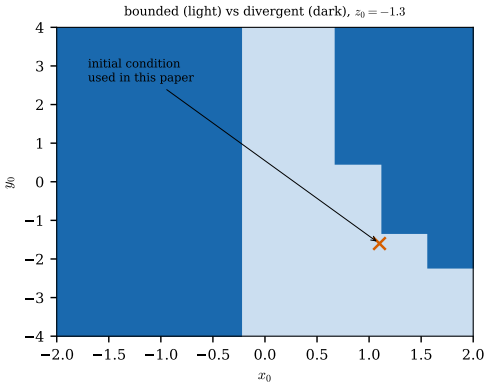

Figure 6: Initial conditions on the slice $z_0 = -1.3$ that remain bounded (light) and that diverge (dark). The cross marks the initial condition used in this paper. 9×9 grid, $h = 0.005$, $t \in [0, 50]$; on this grid the closed-loop map is identical.

the fate of some trajectories near the boundary but, on these grids, neither enlarges nor shrinks the basin appreciably. This is a finite-grid result on one slice, not a statement about the whole basin; it is consistent with the small bound and with the local nature of the sector condition. The result should therefore be read as the suppression of chaotic oscillation within the basin, not as global stabilization.

6 Discussion and conclusion

Deterministic chaos is a testable alternative to exogenous random shocks as an explanation of irregular fluctuations; the stochastic tradition models the same variables as diffusions [11,12], and the two readings differ in whether the irregularity lies in the mechanism or in the noise.

Two of the three equilibria are saddle points of index two, so the necessary condition for a chaotic attractor holds for every commensurate order $\alpha > 0.8863$, yet a sampled scan shows the attractor periodic well above that bound, with a period-doubling cascade between $\alpha = 0.945$ and 0.9575 and the onset of chaos in $(0.9575, 0.965]$. The gap between the analytical bound and the observed onset is the most transferable result of the paper: a condition of this kind is sometimes used in the literature as though it established chaos, and here it does not. At $\alpha = 0.99$ the 0–1 test gives $K = +0.998$ against $K = -0.017$ at $\alpha = 0.9$, and the divergence rate is positive; we rely on the former because the latter ranges from 0.27 to 0.48 depending on the estimation parameters.

Over an ensemble of 20 initial conditions drawn from the attractor, the bounded design reduces the performance index by $98.7\% \pm 1.1\%$ and the integral absolute error by $98.2\% \pm 1.2\%$ on average, not uniformly. For the single initial condition of Tables 5–7, the peak effort is 0.05 and the control energy 3.95×10^{-3}. Both metaheuristics reach the same optimum; their difference, 0.0073% of J, does not survive a change of the search step.

The comparison of Section 5 shows equivalence rather than superiority. A saturated linear-quadratic regulator, obtained in closed form from the same weights, matches the optimized feedback to within 0.03% in J and is marginally better in state cost and integral absolute error. The optimized design is a different route to the same controller: it evaluates the cost on the nonlinear dynamics and uses the

Corrected Proof

linearization only for the local stability constraint, it treats the bound as part of the problem, and it extends unchanged to cost functionals with no closed form. Against active control the factor of six in state cost seen under an unbounded three-input law shrinks to 9% once both are given the same authority.

Five limitations should be stated. The model is a stylized three-state aggregate description without expectations or stochastic shocks, neither calibrated to data nor linked to a concrete policy instrument, so the results hold for the normalized model and the chosen bound, not for an actual economy. The basin of attraction is small and the bounded feedback does not enlarge it on the grids tested, so the result is local suppression of oscillation rather than global stabilization, as the local nature of the sector condition already implies. The design tolerates an implementation delay of at most about a quarter of a time unit, one eighth of the dominant closed-loop period; a slower instrument would require a delay-aware redesign. The metaheuristic solution carries no guarantee of global optimality, and the flat landscape near the optimum means that J is well determined while the gain vector attaining it is not. Finally, only a commensurate order has been considered; the incommensurate case requires (8) with the corresponding M and has been examined for discrete macroeconomic systems in [1], while the extension to the four-dimensional hyperchaotic model of [51], where transient chaos complicates the choice of t_f, is left for future work.

Declaration of competing interest. The authors declare that they have no known competing financial interests or personal relationships that could have appeared to influence the work reported in this paper.

Funding. This research received no specific grant from any funding agency in the public, commercial, or not-for-profit sectors.

Author contributions. Seyed Reza Hejazi: Conceptualization; Methodology; Formal analysis; Supervision; Project administration; Writing — review and editing. **Shaban Mohammadi:** Methodology; Investigation; Writing — original draft. **Mohammad Hossein Seifi:** Software; Validation; Data curation; Visualization. **Elham Dastranj:** Formal analysis; Writing — review and editing. All authors read and approved the final manuscript.

Declaration of generative AI in the preparation of this work. The authors used a large language model (Claude, Anthropic) in two ways: (i) language editing of the manuscript, and (ii) computational support, namely writing verification scripts and checking the numerical values in the text against their output. The research question, the model, the formulation of the control problem and the conclusions are the authors' own. All reported numbers were obtained by running the scripts on the authors' own computer. The authors independently checked all mathematical claims, computational procedures, reported results and their interpretation, and take full responsibility for the content of the manuscript. No generative AI tool is listed as an author.

References

[1] A. Abbes, A. Ouannas, N. Shawagfeh, *An incommensurate fractional discrete macroeconomic system: bifurcation, chaos, and complexity*, Chinese Phys. B **32(3)** (2023) 030203.

[2] O.P. Agrawal, *A general formulation and solution scheme for fractional optimal control problems*, Nonlinear Dynam. **38(1–4)** (2004) 323–337.

Corrected Proof

[3] E. Ahmed, A.M.A. El-Sayed, H.A.A. El-Saka, *Equilibrium points, stability and numerical solutions of fractional-order predator–prey and rabies models*, J. Math. Anal. Appl. **325(1)** (2007) 542–553.

[4] D. Baleanu, Z.B. Güvenç, J.A. Tenreiro Machado (Eds.), *New Trends in Nanotechnology and Fractional Calculus Applications*, Springer, New York, 2010.

[5] H.M. Baskonus, T. Mekkaoui, Z. Hammouch, H. Bulut, *Active control of a chaotic fractional order economic system*, Entropy **17(8)** (2015) 5771–5783.

[6] B. Bodo, A. Mvogo, S. Morfu, *Fractional dynamical behavior of electrical activity in a model of pancreatic β-cells*, Chaos Solit. Fractals **102** (2017) 426–432.

[7] R. Caponetto, G. Dongola, L. Fortuna, I. Petráš, *Fractional Order Systems: Modeling and Control Applications*, World Scientific, Singapore, 2010.

[8] W.-C. Chen, *Nonlinear dynamics and chaos in a fractional-order financial system*, Chaos Solit. Fractals **36(5)** (2008) 1305–1314.

[9] Y.-M. Chu, S. Bekiros, E. Zambrano-Serrano, O. Orozco-López, S. Lahmiri, H. Jahanshahi, A.A. Aly, *Artificial macro-economics: a chaotic discrete-time fractional-order laboratory model*, Chaos Solit. Fractals **145** (2021) 110776.

[10] M.-F. Danca, N. Kuznetsov, *Matlab code for Lyapunov exponents of fractional-order systems*, Internat. J. Bifur. Chaos Appl. Sci. Engrg. **28(5)** (2018) 1850067.

[11] E. Dastranj, S.R. Hejazi, *Exact solutions for Fokker–Planck equation of geometric Brownian motion with Lie point symmetries*, Comput. Methods Differ. Equ. **6(3)** (2018) 372–379.

[12] E. Dastranj, R. Latifi, *A comparison of option pricing models*, Int. J. Financ. Eng. **4(2–3)** (2017) 1750024.

[13] W. Deng, C. Li, J. Lü, *Stability analysis of linear fractional differential system with multiple time delays*, Nonlinear Dynam. **48(4)** (2007) 409–416.

[14] J. Derrac, S. García, D. Molina, F. Herrera, *A practical tutorial on the use of nonparametric statistical tests as a methodology for comparing evolutionary and swarm intelligence algorithms*, Swarm Evol. Comput. **1(1)** (2011) 3–18.

[15] L. Diabi, A. Ouannas, A. Hioual, S. Momani, A. Abbes, *On fractional discrete financial system: bifurcation, chaos, and control*, Chinese Phys. B **33(10)** (2024) 100201.

[16] K. Diethelm, N.J. Ford, A.D. Freed, *A predictor-corrector approach for the numerical solution of fractional differential equations*, Nonlinear Dynam. **29(1–4)** (2002) 3–22.

[17] Y.P. Dousseh, A.V. Monwanou, A.A. Koukpémèdji, C.H. Miwadinou, J.B. Chabi Orou, *Dynamics analysis, adaptive control, synchronization and anti-synchronization of a novel modified chaotic financial system*, Int. J. Dyn. Control **11** (2023) 862–876.

Corrected Proof

[18] A. El-Gohary, I.A. Alwasel, *The chaos and optimal control of cancer model with complete unknown parameters*, Chaos Solitons Fractals **42(5)** (2009) 2865–2874.

[19] L. Fanti, P. Manfredi, *Chaotic business cycles and fiscal policy: an IS-LM model with distributed tax collection lags*, Chaos Solit. Fractals **32(2)** (2007) 736–744.

[20] R. Garrappa, *Numerical solution of fractional differential equations: a survey and a software tutorial*, Mathematics **6(2)** (2018) 16.

[21] D. Guyomar, B. Ducharne, G. Sebald, D. Audigier, *Fractional derivative operators for modeling the dynamic polarization behavior as a function of frequency and electric field amplitude*, IEEE Trans. Ultrason. Ferroelectr. Freq. Control **56(3)** (2009) 437–443.

[22] A.S. Hegazi, E. Ahmed, A.E. Matouk, *On chaos control and synchronization of the commensurate fractional order Liu system*, Commun. Nonlinear Sci. Numer. Simul. **18(5)** (2013) 1193–1202.

[23] H. Jahanshahi, S.S. Sajjadi, S. Bekiros, A.A. Aly, *On the development of variable-order fractional hyperchaotic economic system with a nonlinear model predictive controller*, Chaos Solit. Fractals **144** (2021) 110698.

[24] M.D. Johansyah, A. Sambas, S. Zheng, et al., *Analyzing and controlling chaos phenomena in fractional chaotic supply chain models*, Heliyon **10** (2024) e34703.

[25] D.D. Joshi, S. Bhalekar, P.M. Gade, *Controlling fractional difference equations using feedback*, Chaos Solit. Fractals **170** (2023) 113401.

[26] E. Keshavarz, Y. Ordokhani, M. Razzaghi, *Bernoulli wavelet operational matrix of fractional order integration and its applications in solving the fractional order differential equations*, Appl. Math. Model. **38(24)** (2014) 6038–6051.

[27] D.E. Kirk, *Optimal Control Theory: An Introduction*, Dover, New York, 2004.

[28] N. Laskin, *Fractional market dynamics*, Phys. A **287(3–4)** (2000) 482–492.

[29] Y. Li, Y.Q. Chen, I. Podlubny, *Mittag–Leffler stability of fractional order nonlinear dynamic systems*, Automatica J. IFAC **45(8)** (2009) 1965–1969.

[30] X. Liu, L. Hong, L. Yang, *Fractional-order complex T system: bifurcations, chaos control, and synchronization*, Nonlinear Dynam. **75(3)** (2014) 589–602.

[31] X.J. Liu, L. Hong, L. Yang, et al., *Bifurcations of a new fractional-order system with a one-scroll chaotic attractor*, Discrete Dyn. Nat. Soc. **2019** (2019) 8341514.

[32] D. Matignon, *Stability results for fractional differential equations with applications to control processing*, in: Computational Engineering in Systems and Application Multiconference, Vol. 2, IMACS, IEEE-SMC, Lille, France, 1996, pp. 963–968.

[33] F. Merrikh-Bayat, *More details on analysis of fractional-order Lotka–Volterra equation*, arXiv:1401.0103, 2013.

Corrected Proof

[34] K.S. Miller, B. Ross, *An Introduction to the Fractional Calculus and Fractional Differential Equations*, Wiley, New York, 1993.

[35] K. Moaddy, A. Freihat, M. Al-Smadi, E. Abuteen, I. Hashim, *Numerical investigation for handling fractional-order Rabinovich–Fabrikant model using the multistep approach*, Soft Comput. **22(3)** (2018) 773–782.

[36] A.M. Nagy, N.H. Sweilam, *An efficient method for solving fractional Hodgkin–Huxley model*, Phys. Lett. A **378(30–31)** (2014) 1980–1984.

[37] K.B. Oldham, J. Spanier, *The Fractional Calculus*, Academic Press, New York, 1974.

[38] I. Petráš, *A note on the fractional-order Volta's system*, Commun. Nonlinear Sci. Numer. Simul. **15(2)** (2010) 384–393.

[39] I. Petráš, *Fractional-Order Nonlinear Systems: Modeling, Analysis and Simulation*, Springer, Berlin, 2011.

[40] K. Sasakura, *On the dynamic behavior of Schinasi's business cycle model*, J. Macroecon. **16(3)** (1994) 423–444.

[41] N.H. Sweilam, A.M. Nagy, A.A. El-Sayed, *Second kind shifted Chebyshev polynomials for solving space fractional order diffusion equation*, Chaos Solitons Fractals **73** (2015) 141–147.

[42] V.V. Tarasova, V.E. Tarasov, *Logistic map with memory from economic model*, Chaos Solit. Fractals **95** (2017) 84–91.

[43] M.S. Tavazoei, M. Haeri, *A necessary condition for double scroll attractor existence in fractional-order systems*, Phys. Lett. A **367(1–2)** (2007) 102–113.

[44] M.S. Tavazoei, M. Haeri, *Chaotic attractors in incommensurate fractional-order systems*, Phys. D **237(20)** (2008) 2628–2637.

[45] M.S. Tavazoei, M. Haeri, M. Attari, S. Bolouki, M. Siami, *More details on analysis of fractional-order Van der Pol oscillator*, J. Vib. Control **15(6)** (2009) 803–819.

[46] M.S. Tavazoei, M. Tavakoli-Kakhki, F. Bizzarri, *Nonlinear fractional-order circuits and systems: motivation, a brief overview, and some future directions*, IEEE Open J. Circuits Syst. **1** (2020) 220–232.

[47] Z. Wang, X. Huang, G. Shi, *Analysis of non-linear dynamics and chaos in a fractional-order financial system with time delay*, Comput. Math. Appl. **62(3)** (2011) 1531–1539.

[48] B. Wang, J. Liu, M.O. Alassafi, F.E. Alsaadi, H. Jahanshahi, S. Bekiros, *Intelligent parameter identification and prediction of variable time fractional derivative and application in a symmetric chaotic financial system*, Chaos Solit. Fractals **154** (2022) 111590.

[49] A. Wolf, J.B. Swift, H.L. Swinney, J.A. Vastano, *Determining Lyapunov exponents from a time series*, Phys. D **16(3)** (1985) 285–317.

Corrected Proof

[50] B. Xu, X. Ye, G. Wang, Z. Huang, C. Zhang, *A fractional-order improved quantum logistic map: chaos, 0–1 testing, complexity, and control*, Axioms **12(1)** (2023) 94.

[51] A. Yousefpour, H. Jahanshahi, J.M. Munoz-Pacheco, S. Bekiros, Z. Wei, *A fractional-order hyper-chaotic economic system with transient chaos*, Chaos Solit. Fractals **130** (2020) 109400.

Corrected Proof